Supporting Information

Two Coexisting Liquid Phases in Switchable Ionic Liquids

Juan Yao,[§] David B. Lao,[†,‡] Xiao Sui,[§,‡] Yufan Zhou,[#,‡] Satish K. Nune,[†] Xiang Ma,[‖], Tyler P. Troy,[⊥]
Musahid Ahmed,[⊥] Zihua Zhu,[#] David J. Heldebrant,[†] and Xiao-Ying Yu[,§]*

[§] Earth and Biological Sciences Directorate, Pacific Northwest National Laboratory, Richland, WA 99354 (USA).

[†] Energy and Environment Directorate, Pacific Northwest National Laboratory, Richland, WA 99352 (USA).

[#] W. R. Wiley Environmental Molecular Science Laboratory, Pacific Northwest National Laboratory, Richland, WA 993524 (USA).

[‖] Dept. Chemistry, Idaho State University, Pocatello, ID 83209 (USA)

[⊥] Chemical Sciences Division, Lawrence Berkeley National Laboratory, Berkeley, CA, 94720, USA

*Corresponding author electronic mail: xiaoying.yu@pnnl.gov

Additional experimental details are provided below.

Experimental Details

Ionic liquid preparation

All synthetic procedures were performed in a nitrogen-filled glovebox. 1,8-Diazabicycloundec-7-ene (DBU) purchased from Acros was dried, distilled over sodium metal (Na^0), and degassed prior to bringing into the glovebox filled with Ar or N_2. Anhydrous 1-hexanol was purchased from Acros and used without further purification. Supercritical fluid 99.999% extraction grade carbon dioxide (CO_2) was purchased from Praxair and plumbed directly into the glovebox. In a typical experiment, the SWIL solvent is prepared using DBU, 1-hexanol, and carbon dioxide. For partial ionic solutions, a 1:1 equivalent (by mole) solution of dry, air-free DBU and 1-hexanol was mixed in a glass vial. The clear, colorless solution was sparged with CO_2 until the desired mass uptake (percent ionic character) was achieved. Per 1.0 g of DBU and 1-hexanol solution, 0.043 g, 0.086 g, and 0.130 g CO_2 was loaded for 25%, 50%, and 75% ionic character. The mass uptake was determined by periodically weighing the solution.[1] For fully ionic solution, the DBU and 1-hexanol mixture was stirred overnight in a Parr reactor pressurized under 300 psi of CO_2. The SWIL solutions were immediately loaded into the SALVI cells for analysis.

The microchannel in SALVI was thoroughly washed by ethanol or methanol prior to usage. The SWILs with different loadings of CO_2 (0%, 25%, 50%, 75% and 100%) were injected into individual microfluidic devices in an Ar or N_2 glove box.

SALVI fabrication

The details of vacuum compatible microfluidic reactor, namely, System for Analysis at the Liquid Vacuum Interface (SALVI) fabrication can be found in our previous publications.[2-4] Briefly, soft lithography was applied to make a 200 µm wide by 300 µm deep channel on a silicon wafer as the microfluidic mold. Polydimethylsiloxane (PDMS) was filled in the mold to form the block with the channel after it is hardened. A 100 nm thick SiN membrane window supported on a silicon frame (frame size 7.5×7.5 mm^2, window size 1.5×1.5 mm^2, Norcada) was bonded to the PDMS block by oxygen plasma treatment. The two pieces were attached to each other by immediate contact to seal the microchannel and form the detection area.

ToF-SIMS imaging

ToF-SIMS V spectrometer (IONTOF GmbH, Münster, Germany) was employed for *in situ* liquid SIMS analysis of SWILs. In this study, a 25 keV Bi_3^+ cluster ion beam was applied as the primary ion beam. During the measurement, the Bi_3^+ beam made an aperture with 2 µm in diameter. The pulse width of ~180 ns was used for sputtering through the SiN membrane. After punch-through, the ion beam bombarded on the sample surface for about 200 s and then the pulse width was changed to 80 ns to obtain better mass resolution. The maximum chamber pressure during analysis was 8.4×10^{-7} mbar, indicating that there was no spraying or fast spreading of aqueous solutions from the aperture occurred.[3] Before SIMS analysis, a 1 KeV O_2^+ beam was scanned on the SiN window for ~20 s to remove surface contamination. Also, an electron flood gun was used to compensate surface charging during all measurements. A total measurement time is 400 s after punch-through. The raster resolution is 32×32 pixels. The same instrument settings were applied to all the samples measurement. The mass resolution was approximately 500 in the positive mode and 370 in the negative mode, based on the half peak width of the peak Si^+ (m/z^+ 28) and CN^- (m/z^- 26), respectively.[5]

Figure 1b provides the cross-sectional view of the sample in a 200 µm-wide SALVI when it was analyzed using liquid ToF-SIMS. The critical step of liquid ToF-SIMS measurement is the size of the aperture, which is 2 µm in diameter, so the liquid can be hold within the channel due to the surface tension after being punched through. The schematic depth profile in **Figure** 1c represents the period

before the ion beam punching through the SiN window (region I) by the primary ion beam Bi_3^+, during the punching through (region II), after punching through (region III and IV). In region III, a relatively high current of ion beam was applied in order to obtain high intensity for two dimensional (2D) and three dimensional (3D) images reconstruction, shown in **Figures** 1e and f; while in region IV, a lower current was applied to acquire better resolution for mass spectra, exemplified in **Figure** 1d.

SIMS Data analysis

All data were analyzed with IONTOF software (SurfaceLab, version 6.3). Mass spectra were calibrated using Si^+, $SiCH_3^+$, $SiC_3H_9^+$, $Si_3C_5H_{15}O_3^+$, $Si_4C_7H_{21}O_4^+$, and Bi^+ peaks for positive spectra; CH^-, $C_6H_{13}O^-$, and $C_7H_{13}O_3^-$ peaks for negative spectra, respectively.[6] OriginPro 2015 was employed for plotting the spectra. For spectral PCA, selected unit mass peaks were used and MATLAB R2012a (MathWorks, Natick, MA, USA) was employed for the analysis.[6] The peaks were selected based on the following three criteria: 1) the intensity of the peak is greater than 0.3% of total ion intensity in each mode; 2) the intensity of the peak is three times higher than its adjacent peaks; 3) peaks that are relevant to the study. Before running spectral PCA, data was pretreated by normalization to the total intensities of all the selected peaks, square root transformation, and mean centering.[7]

AFM imaging

AFM AC mode images were obtained using a MFP3D AFM (Asylum Research). Measurements were performed in air at room temperature using SuperSharpSilicon probes (SSS-NCH, Olympus). Images were analyzed using Igor Pro 6.12 software (WaveMetrics).

VUV SPI-MS

The fully CO_2 exposed SWIL (100%) was loaded in the SALVI and analyzed by a reflectron time-of-flight mass spectrometer (ReToF-MS). This ReToF-MS was coupled to a three meter vacuum ultraviolet (VUV) monochromator at the Chemical Dynamics Beamline (9.0.2) at the Advanced Light Source in Lawrence Berkeley National Laboratory (LBNL).[8] This apparatus enables single photon ionization (SPI) representing "soft ionization" which significantly reduces secondary ions or multiphoton ionization events. Two 2 µm holes were pre-milled using the Focused Ion Beam and Scanning Electron Microscope (FIB/SEM) on the SiN membrane window. The mass spectra were collected for photon energies ranging between 8.0 and 11.0 eV with intervals 0.1 eV. The mass spectrum obtained at 10.5 eV is presented to provide the characteristic DBU peak detected by VUV SPI-MS. Other details in the integration and experimental results are being prepared in another manuscript.

Supplemental Figures
The following figures are provided to substantiate the results and discussion section.
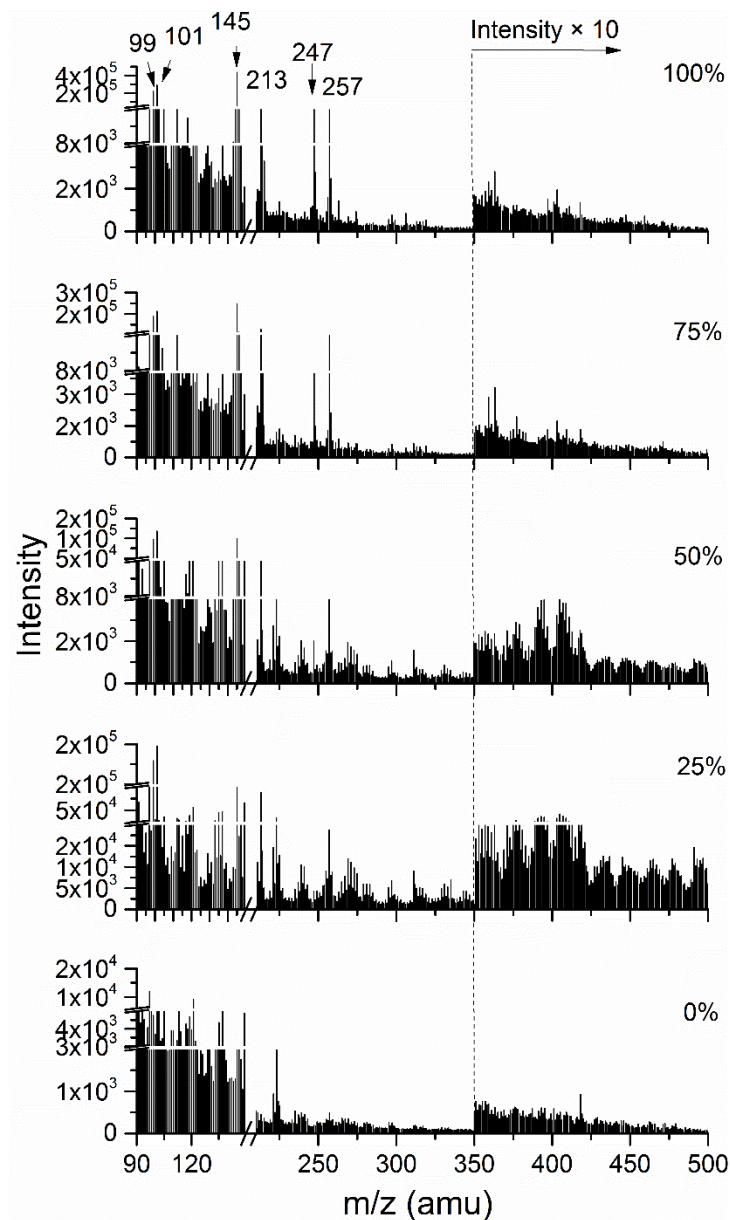
Figure S1. Negative ToF-SIMS spectra (m/z⁻ 90-500) showing comparisons of SWILs loaded with 0%, 25%, 50%, 75%, and 100% CO_2.

The ToF-SIMS can detect the positive and negative ions. **Figure S1** depicts comparative negative ion mass spectra of the SWILs with different CO_2 loading. Combining with Table 1, we identified the deprotonated 1-hexanol fragment (m/z⁻ 99)[9], 1-hexanol (m/z⁻ 101), hexylcarbonate (m/z⁻ 145), CO_2-bonded negative ions (m/z⁻ 213, 257) and 1-hexanol dimer (m/z⁻ 247). ⁻ These results are in accordance with the previous publication regarding these characteristic components including hexylcarbonate and protonated DBU zwitterion.[10] More importantly, the observation of other key species (m/z⁻ 99,145) confirms that the glassy phase and solvent phase are coexisting in the CO_2 loaded SWILs.[11]
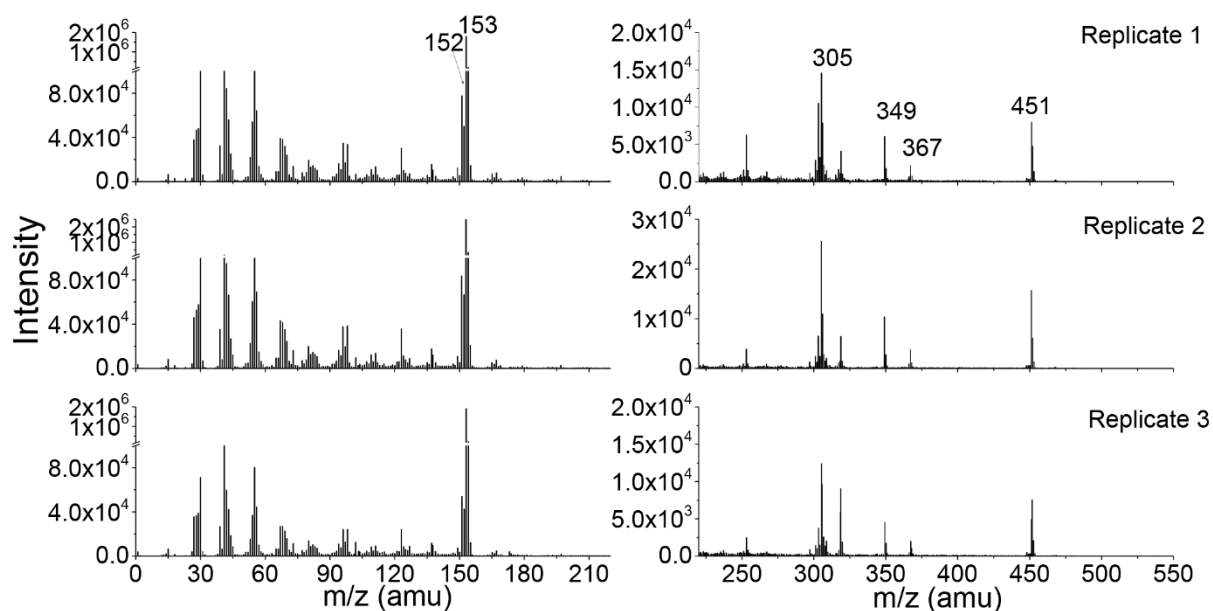
Figure S2. SIMS positive mass spectral comparison of key m/z peaks at different replicate locations in the 100% CO_2 loaded sample.

Figure S2 presents the positive mass spectra of three replicates of the 100% CO_2 loaded SWIL. The intensities of the key components identified in Table 1 are consistent in these measurements. This confirms the data reproducibility and the existence of these characteristic ionic clusters and dimers in SWILs.
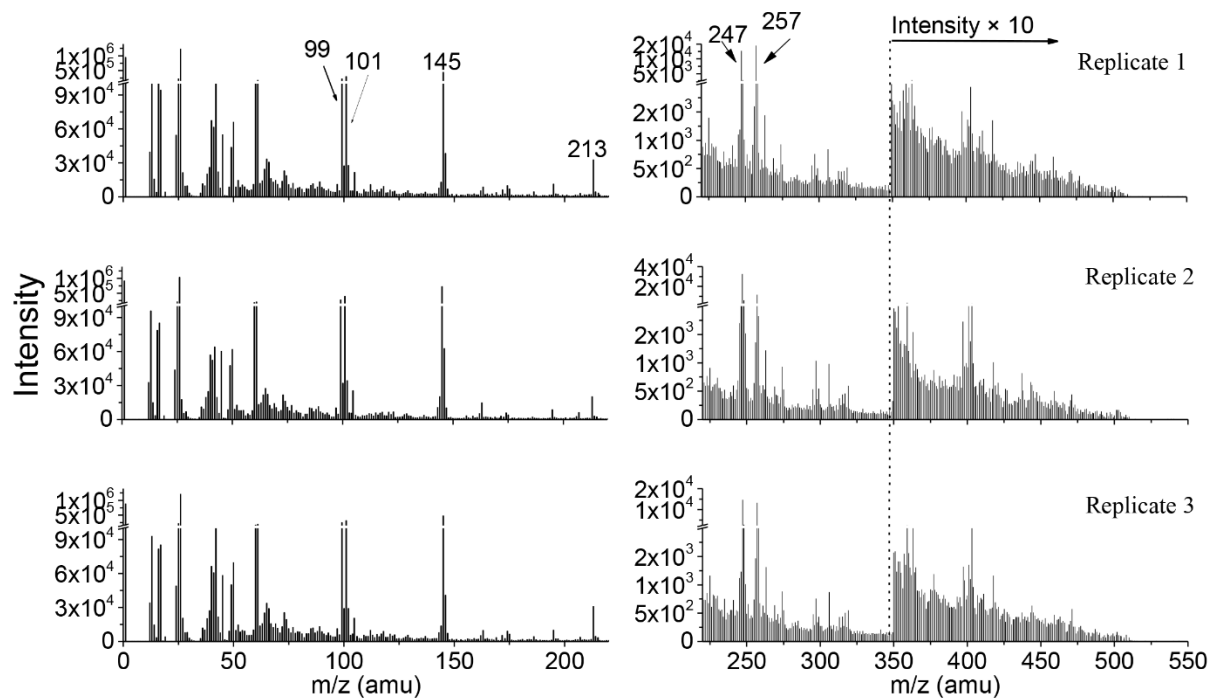
Figure S3. SIMS negative mass spectral comparison of key m/z peaks at different replicate locations in the 100% CO_2 loaded sample.

Figure S3 presents the negative mass spectra of three replicates of the 100% CO_2 loaded SWIL. The intensities of the key components identified in Table 1 are consistent in these measurements. This again confirms the data quality and reproducibility as well as the existence of these characteristic molecular ions and ionic clusters and ion pairs in the SWIL.
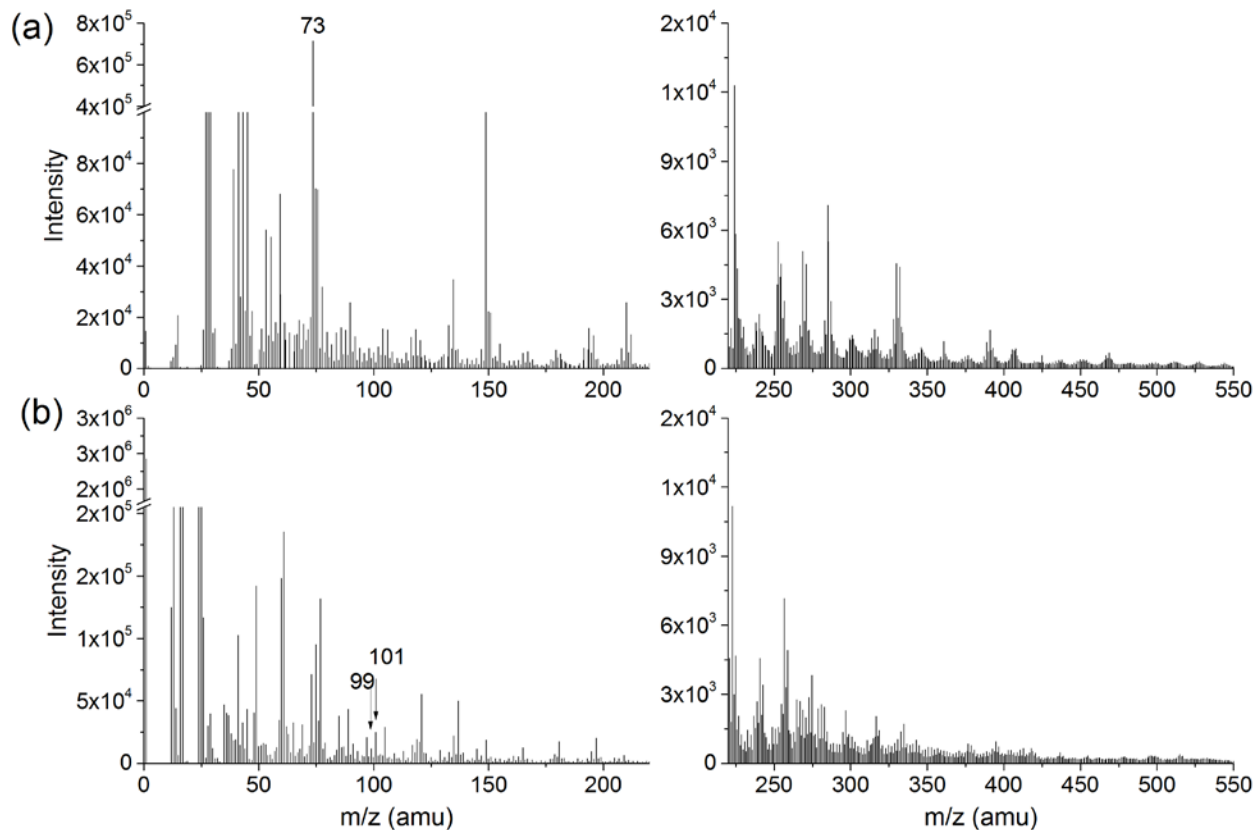
Figure S4. (a) Positive mass spectrum of 1-hexanol (m/z$^+$ 0-550). (b) Negative mass spectra of 1-hexanol (m/z$^-$ 0-550).

Figure S4 presents the positive (a) and negative (b) mass spectra of 1-hexanol. In the positive mode, the prominent peak m/z$^+$ 73 (SiC$_3$H$_9$$^+$) represents the PDMS fragment ion.[12] In the negative mode of the mass spectrum, fragment ions of 1-hexanol (m/z$^-$ 99) and deprotonated 1-hexanol (m/z$^-$ 101) were observed.
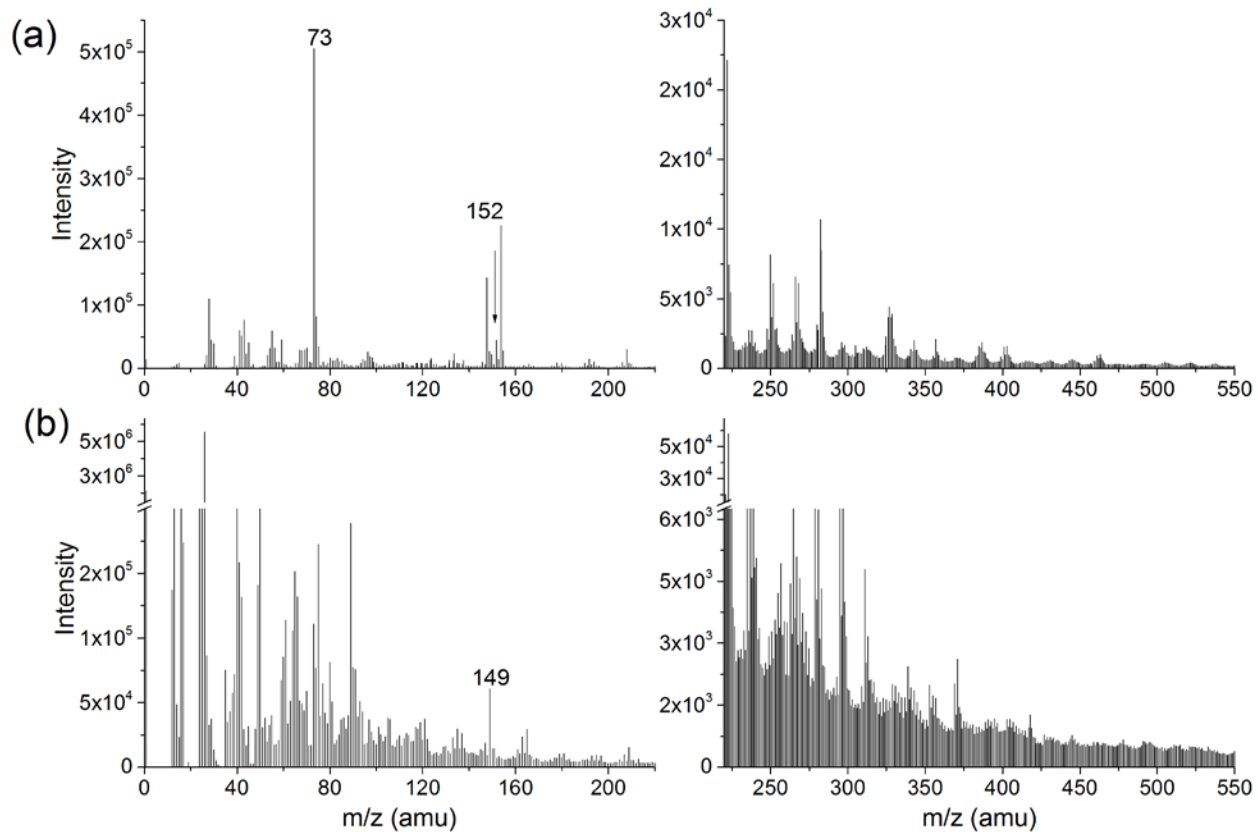
Figure S5. (a) Positive mass spectrum of DBU (m/z$^+$ 0-550). (b) Negative mass spectrum of DBU (m/z$^-$ 0-550).

Figure S5 presents the positive (a) and negative (b) mass spectra of DBU. In the positive mode, the PDMS fragment ion (m/z$^+$ 73) and the peak DBU$^+$ (m/z$^+$ 152) were observed. The prominent peak m/z$^-$ 149 (Si$_2$C$_3$H$_9$O$_3^-$) in the negative mass spectra is a PDMS fragment ion.[13]
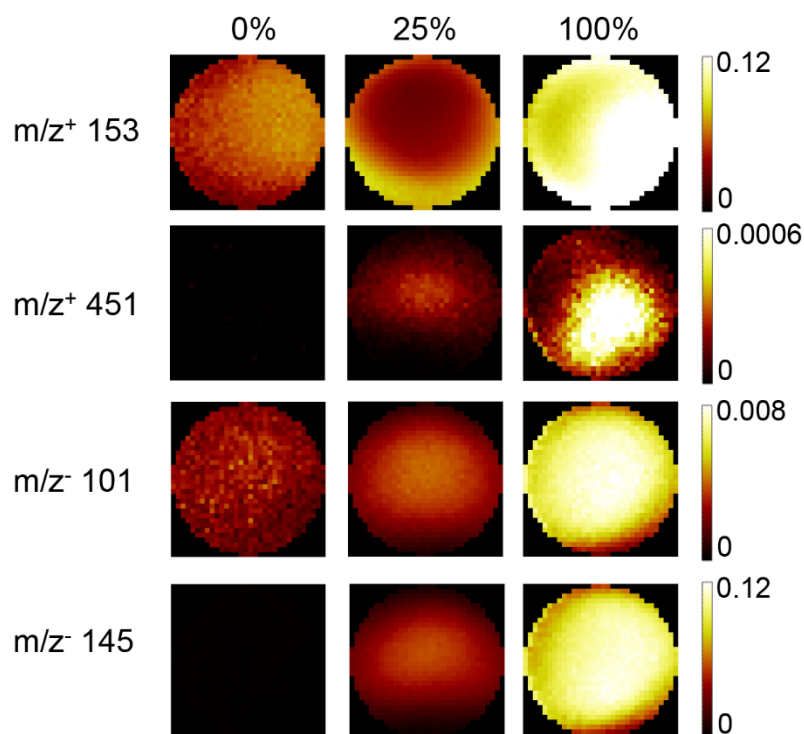
Figure S6. Comparison of 2D reconstructed images of positive peaks m/z$^+$ 153 and 451, negative peaks m/z$^-$ 101 and 145 in 0%, 25% and 100% CO_2 loaded samples.

To visualize the differences between the ionic and non-ionic liquids in terms of ionic chemical species, **Figure S6** compares the reconstructed two dimensional (2D) images of key ionic peaks m/z$^+$ 153, 451 in positive mode and m/z$^-$ 101, 145 in negative mode in the non-ionic sample (0%) and CO_2 loaded SWILs (25% and 100%). Each image was normalized to the total intensities acquired from the corresponding sample. The color scale was adjusted to be identical for the same chemical species, with dark red representing low intensity and bright yellow representing high intensity. The comparison demonstrates that the ionic chemical species are more abundant in the CO_2 loaded SWILs, especially in the 100% fully CO_2 loaded one. It has been the first spatial chemical mapping of SWILs in 2D imaging, providing a new approach to analyze the SWILs.
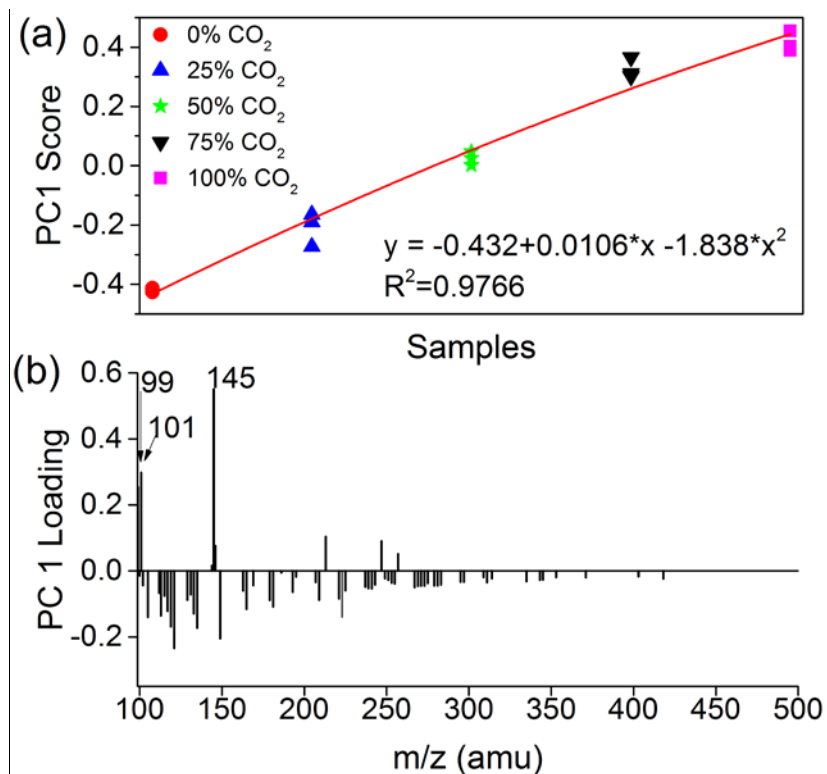
Figure S7. PCA results of selected peaks from five samples in negative mode (a) a plot of the PC1 score versus CO_2 loading percentage of SWIL and non-ionic liquid samples, the solid line is the least squares fit using a polynomial function, (b) corresponding PC 1 loading

The intensity of individual peaks was normalized to total selected ions intensities in spectral PCA before squared root transformation and mean centering pretreatment. As shown in **Figure S7a**, PC 1 separates the SWIL samples loaded with 50%, 75% and 100% CO_2 from the 0% and 25% CO_2 loaded SWILs. Together with the results displayed in **Figure S7b**, the peaks m/z$^-$ 99, 101, and 145 contribute to the distribution of highly CO_2 loaded SWILs (50%, 75% and 100%) in the positive PC1. The highly loaded CO_2 SWILs have more ionic peaks, including solvents (e.g., m/z$^-$ 99, 101), and hexylcarbonate (m/z$^-$ 145). Additionally, the fitting plot shows the PC1 score versus the percentage of loaded CO_2 in all samples. The PC1 scores are polynomial correlated to the CO_2 loading percentage. The fitting results could provide the relationship regarding the relative composition of the samples' surface and the amount of CO_2 loaded into the SWILs. Therefore, one can use the fitting curve to estimate the CO_2 contents captured by the DBU and 1-hexanol SWIL.
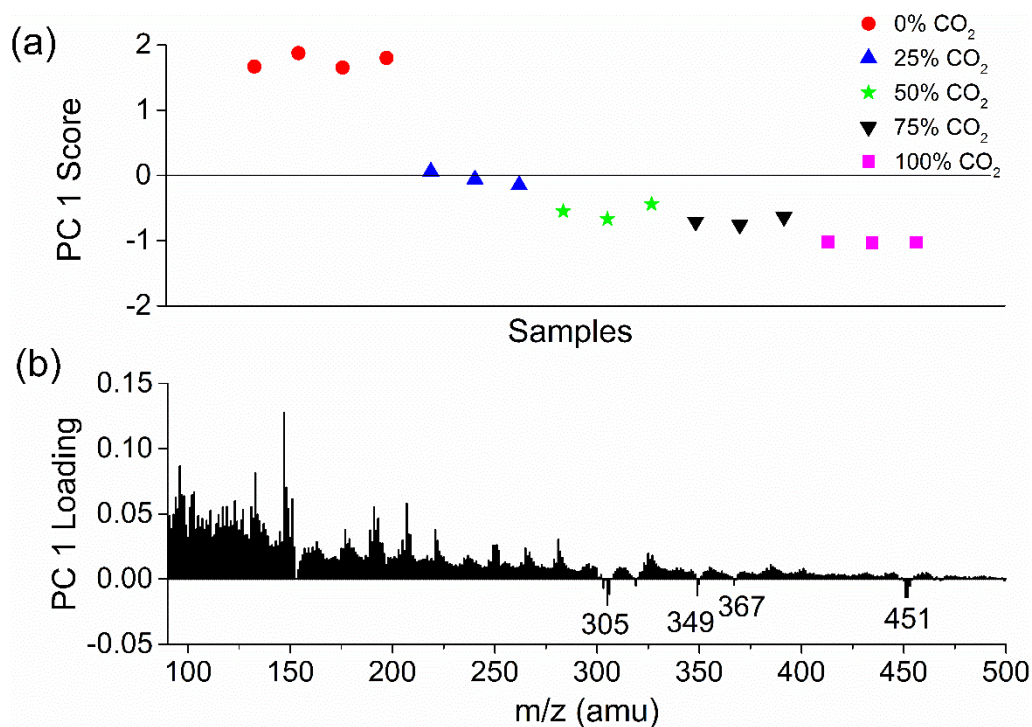
Figure S8. (a) Positive spectral PC1 score plot and (b) PC1 loadings using all positive peaks. Peaks are normalized to the intensity of DBU molecular ion, m/z^+ 153.

Figure S8 provides a similar distribution of score trend of the five SWIL samples compared to the results in **Figure 3**, although different data pretreatment method and peak selections were used. PC1 explains 95% of variance. This finding indicates that results presented in Fig. 3 capture the essence of the data set.
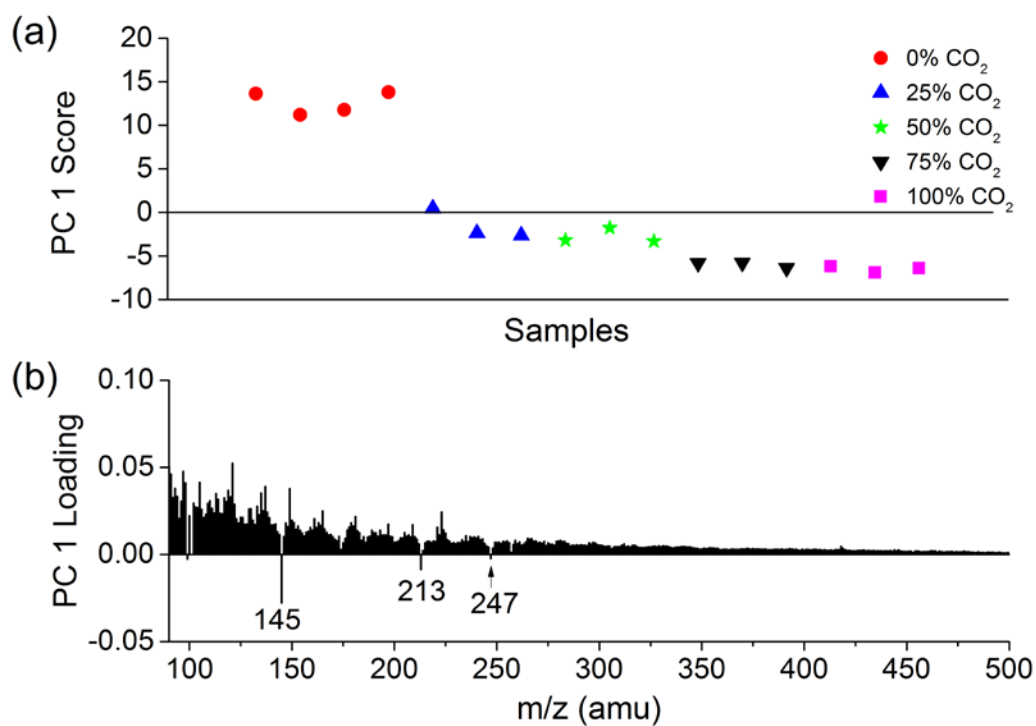
Figure S9. Spectral PCA score plot (a) and loadings (b) using all negative peaks. Peaks are normalized to the molecular ion of 1-hexanol, m/z⁻ 101.

Despite of the different data pretreatment methods and inclusion of all peaks, **Figure S9** provides a similar distribution of all five SWIL samples in the PC1 score plot to the results in **Figure S7**. PC 1 explains 98% of variance. This result and along with the analysis in Figure S8 further confirm that the spectral PCA results presented in the main text are consistent and reliable.
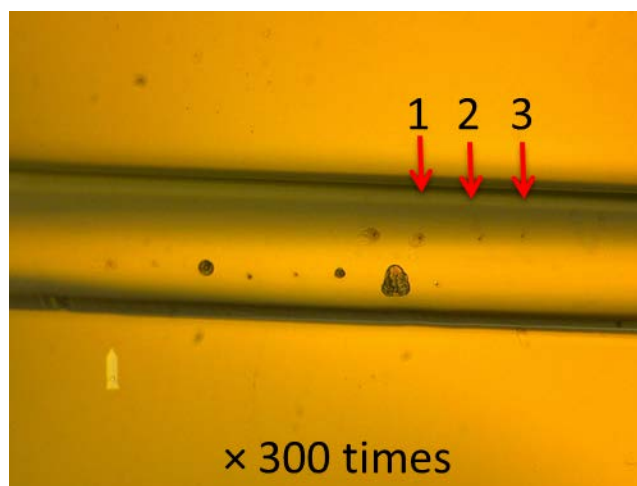
Figure S10. Positive replicate data points analyzed using 100% CO_2 sample.

Figure S10 presents the 300-time magnified optical microscope image of the microfluidic channel that was used to analyze the SWIL loaded with 100% CO_2. The depth profile data obtained from the three replicate data points indicated in this figure were analyzed for reconstructing 3D images in **Figure 4**.
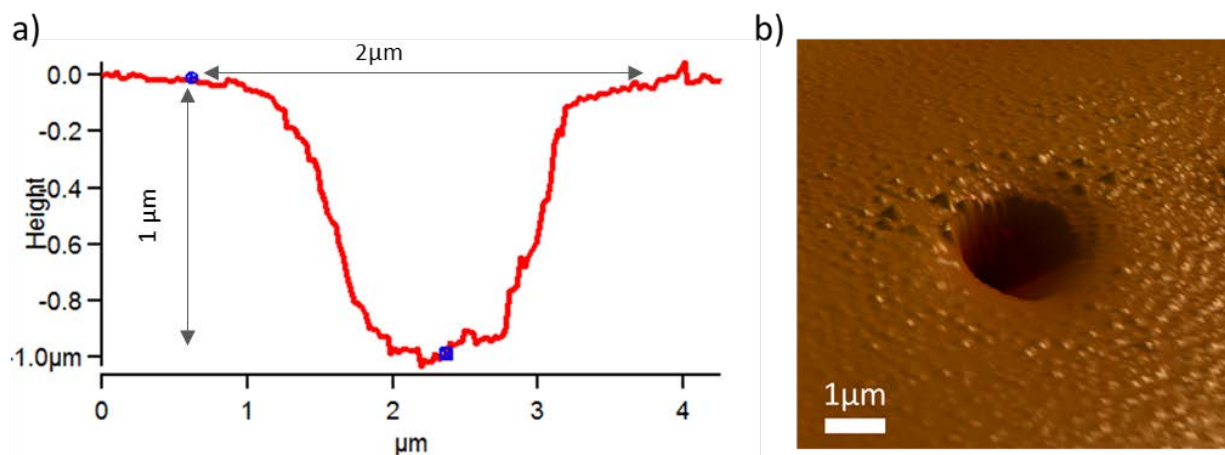
Figure S11. a) AFM image of the crater depth in the measured 100% SWIL in the SALVI microfluidic channel. b) The topographic image of the crater using AFM.

Since our ToF-SIMS was not equipped with *in situ* tomography and depth measurement capabilities, correlative imaging with atomic force microscopy (AFM) was conducted to determine the crater depth in the sample after SIMS measurements. The total depth of the hole, including the 100 nm thick SiN membrane and the depth of the crater into the cell, was determined to be 1 μm (**Figure S11a**). The AFM image of the crater surface was provided in **Figure S11b**. The diameter of the hole is approximately 2 ☐m. The AFM measurement provided additional evidence that the SWIL was probed using the dynamic ToF-SIMS approach. Here a uniform sputtering rate was assumed throughout depth profiling.
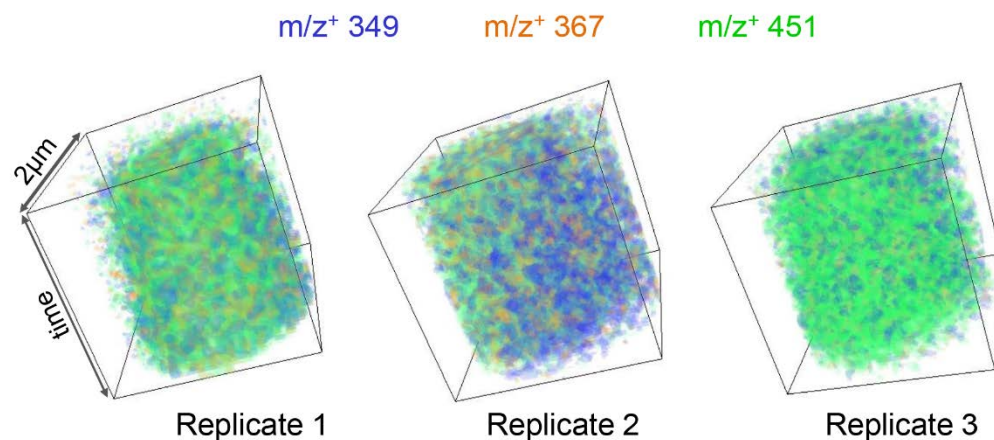
Figure S12. 3D Images of selected positive peaks in different replicate points of 100% CO_2 loaded sample.

Figure S12 presents the 3D overlay images of three selected positive ion signals at different replicate data points of the 100% CO_2 loaded sample. Ion clusters (m/z$^+$ 367 and 451) and the neutral molecule attached ions (m/z$^+$ 349) are not homogeneous as that of IL and two liquid phases coexist. This figure confirms that the heterogeneous distribution of these ion clusters is ubiquitous rather than a unique case obtained from a single data point.
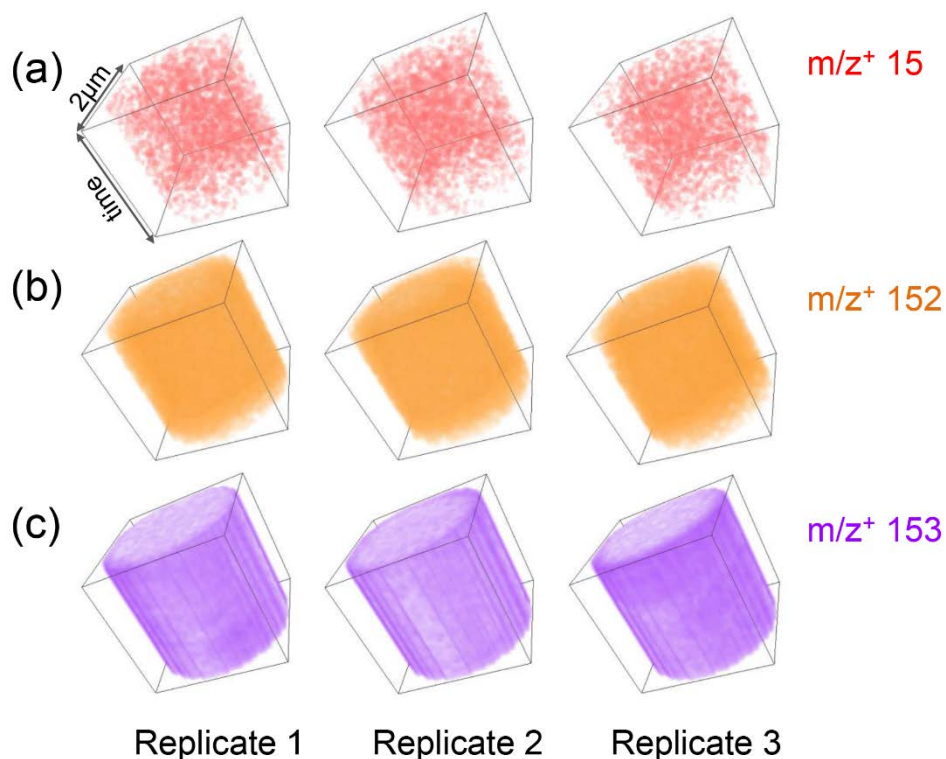
Figure S13. Reconstructed 3D images of (a) CH_3^+ (m/z^+ 15), (b) DBU^+ (m/z^+ 152), and (c) protonated $DBUH^+$ (m/z^+153) in the 100% CO_2 loaded SWIL sample.

Figure S13 provides reference 3D images for **Figure 4**. The distribution of the CH_3^+ (m/z^+ 15) (Figure S12a), DBU^+ (m/z^+ 152) (Figure S12b), and $DBUH^+$ (m/z^+ 153) (Figure S12c) at different replicate locations is homogeneous compared to the spatial distribution of the peaks m/z^+ 349, 367 and 451 at the corresponding locations. The homogeneous distribution of the CH_3^+ in the sample confirms that the heterogeneity of the ionic liquids is attributed to the SWIL's intrinsic chemical nature, not the SIMS instrumental artifact. In addition, the even distribution of DBU^+ and $DBUH^+$ (m/z^+ 152 and 153) indicates that there are indeed two liquid phases in the SWILs.
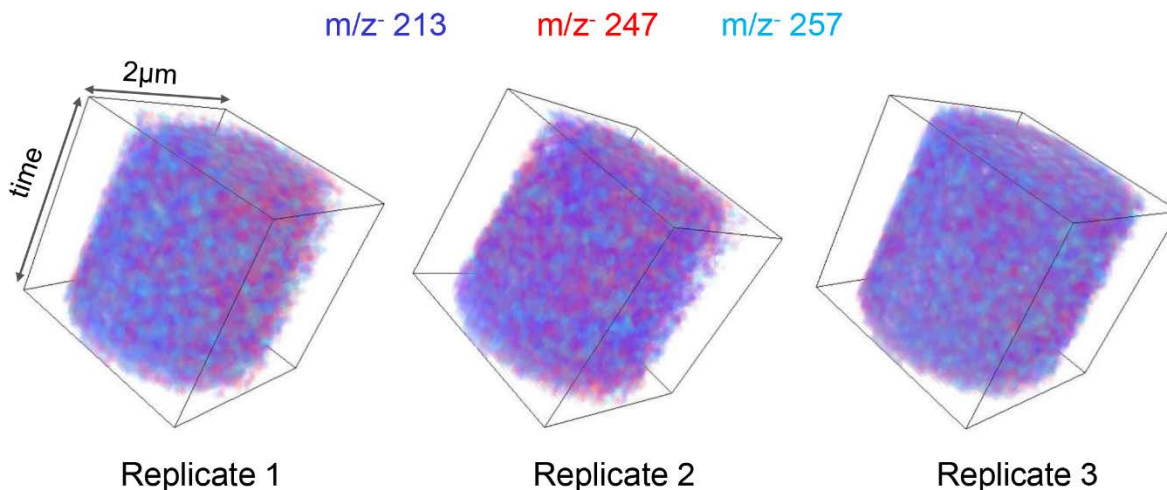
Figure S14. 3D Images of selected negative peaks at different replicate points of the 100% CO_2 loaded sample. Dark blue represents m/z⁻ 213, red m/z⁻ 247 and aqua blue m/z⁻ 257.

Figure S14 presents the 3D overlay images of two selected negative ion signals at different replicate data points of the 100% CO_2 loaded sample. CO_2 attached ions (m/z⁻ 213) by van der Waals force and CO_2-bond cluster ions (m/z⁻ 247, 257) are not evenly distributed. This observation suggests that the SWIL solvent structure is not homogeneous as that of IL and two liquid phases coexist. This result is consistent with what was illustrated in the positive ion 3D images.
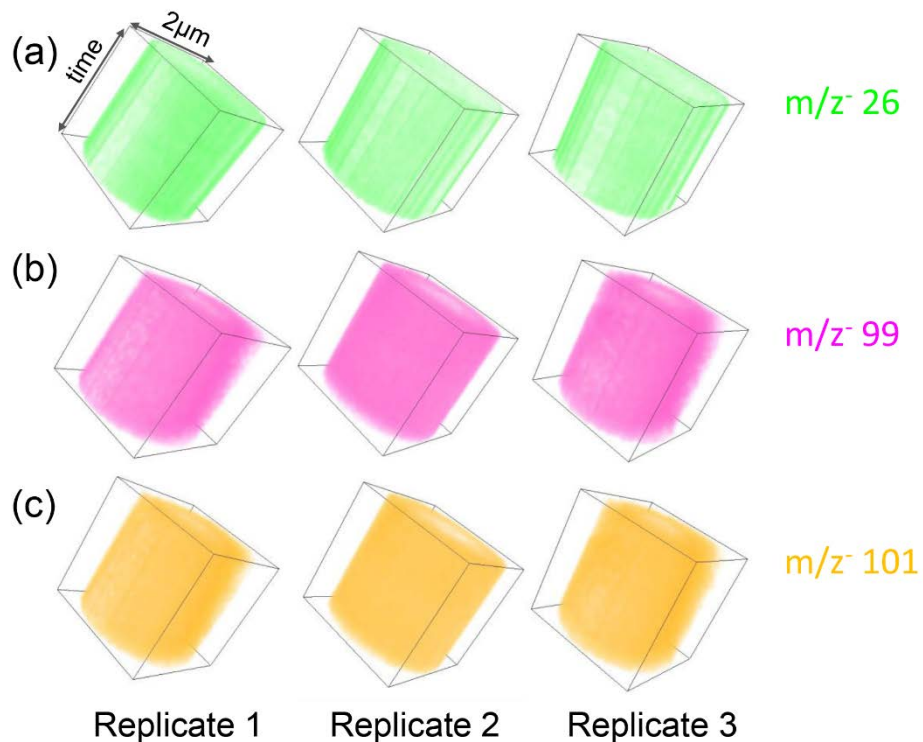
Figure S15. Reconstructed 3D images of (a) CN⁻ (m/z⁻ 26), (b) 1-hexanol fragment (m/z⁻ 99), and (c) deprotonated 1-hexanol (m/z⁻ 101) in the 100% CO_2 loaded SWIL sample.

Figure S15 provides reference 3D images for Figure S13. The distribution of the CN⁻ (m/z⁻ 26), 1-hexanol fragment (m/z⁻ 99), and deprotonated 1-hexanol (m/z⁻ 101) in the different punch-through replicate points is relatively homogeneously, compared to the spatial distribution of the peaks m/z⁻ 213 and 247 in the corresponding punch-through replicate points. The homogeneous distribution of the CN⁻, 1-hexanol (m/z⁻ 99 and 101) in the sample confirms that the heterogeneity of the ionic liquids is attributed to the SWIL's intrinsic chemical nature, not the SIMS instrumental artifact.
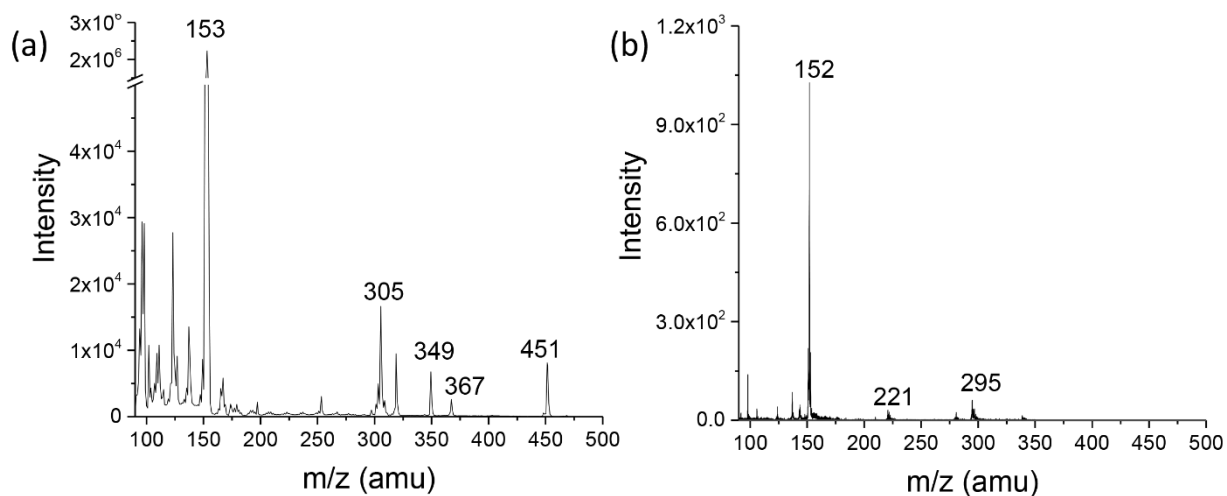
Figure S16. The comparison of the mass spectra of 100% CO_2 loaded SWIL acquired from ToF-SIMS (a) and VUV SPI-MS (b).

Figure S16 depicts the comparison of the positive mode mass spectra of 100% CO_2 loaded SWIL analyzed using ToF-SIMS (a) and Vacuum Ultraviolet (VUV) Single-Photon Ionization Mass Spectrometry (SPI-MS) (b). The major prominent peak observed in the ToF-SIMS is protonated DBU (m/z^+ 153), and the dominant peak acquired from SPI-MS corresponds to DBU with positive charge (m/z^+ 152). The SPI MS result provides the complementary experimental evidence that helps confirm the identification of the protonated DBU (m/z^+ 153) observed in the ToF-SIMS.

Supplemental Table

Table S1 lists the identification of the peaks detected in the positive mode of ToF-SIMS and VUV SPI-MS.

Table S1. Key peaks and possible identification observed in ToF-SIMS and VUV SPI-MS in the positive mode.

m/z (amu)	possible identification	ToF-SIMS	m/z (amu)	possible identification	VUV SPI-MS	references
153	$C_9H_{17}N_2^+$	$[DBU+H]^+$	152	$C_9H_{16}N_2^+$	DBU^+	
305	$C_{18}H_{33}N_4^+$	$[DBU+H]^+ \bullet DBU$	221	$Si_3C_7H_{21}O_2^+$	$[(SiOC_2H_6)_2(SiOC_2H_5)]^+$	[14]
349	$C_{19}H_{33}N_4O_2^+$	$[DBU+H]^+ \bullet DBU \bullet CO_2$	295	$Si_4O_3C_9H_{27}^+$	$[(SiOC_2H_6)_3Si(CH_3)_3]^+$	[15]
367	$C_{19}H_{35}N_4O_3^+$	$2[DBU+H]^+ [HCO_3]^-$				
451	$C_{25}H_{47}N_4O_3^+$	$2[DBU+H]^+[C_6H_{13}OCO_2]^-$				

References
1.   Heldebrant, D. J.; Yonker, C. R.; Jessop, P. G.; Phan, L., Organic Liquid CO2 Capture Agents with High Gravimetric CO2 Capacity. *Energy Environ. Sci.* **2008,** *1*, 487-493.
2.   Yu, X.-Y.; Yang, L.; Cowin, J.; Iedema, M.; Zhu, Z. Systems and Methods for Analyzing Liquids under Vacuum. 8,555,710, Oct. 15., 2013, 2013.
3.   Yang, L.; Yu, X.-Y.; Zhu, Z.; Iedema, M. J.; Cowin, J. P., Probing Liquid Surfaces under Vacuum Using SEM and ToF-SIMS. *Lab Chip* **2011,** *11*, 2481-2484.
4.   Yang, L.; Yu, X.-Y.; Zhu, Z.; Thevuthasan, T.; Cowin, J. P., Making a Hybrid Microfluidic Platform Compatible for in situ Imaging by Vacuum-based Techniques. *Title J. Vac. Sci. Technol., A* **2011,** *29*, 061101.
5.   Yao, J.; Zhou, Y.; Sui, X.; Lao, D.; Heldebrant, D.; Zhu, Z.; Yu, X.-Y., Switchable 1,8-Diazabicycloundec-7-ene and 1-Hexanol Ionic Liquid Analyzed by Liquid ToF-SIMS. *Surf. Sci. Spectra* **2016,** *23*, 9-28.
6.   Green, F. M.; Gilmore, I. S.; Seah, M. P., TOF-SIMS: Accurate Mass Scale Calibration. *J. Am. Soc. Mass Spectrom.* **2006,** *17*, 514-523.
7.   Graham, D. J.; Wagner, M. S.; Castner, D. G., Information from Complexity: Challenges of TOF-SIMS Data Interpretation. *Appl. Surf. Sci.* **2006,** *252*, 6860-6868.
8.   Parker, D. S. N.; Kaiser, R. I.; Troy, T. P.; Ahmed, M., Hydrogen Abstraction/Acetylene Addition Revealed. *Angew. Chem.* **2014,** *126*, 7874-7878.
9.   Zhou, Y.; Yao, J.; Ding, Y.; Yu, J.; Hua, X.; Evans, J. E.; Yu, X.; Lao, D. B.; Heldebrant, D. J.; Nune, S. K.; Cao, B.; Bowden, M. E.; Yu, X.-Y.; Wang, X.-L.; Zhu, Z., Improving the Molecular Ion Signal Intensity for In Situ Liquid SIMS Analysis. *J. Am. Soc. Mass Spectrom.* **2016,** 1-8.
10.   Jessop, P. G.; Heldebrant, D. J.; Li, X.; Eckert, C. A.; Liotta, C. L., Green Chemistry: Reversible Nonpolar-to-polar Solvent. *Nature* **2005,** *436*, 1102-1102.
11.   Cantu, D. C.; Lee, J.; Lee, M.-S.; Heldebrant, D. J.; Koech, P. K.; Freeman, C. J.; Rousseau, R.; Glezakou, V.-A., Dynamic Acid/Base Equilibrium in Single Component Switchable Ionic Liquids and Consequences on Viscosity. *J. Phys. Chem. Lett.* **2016,** *7*, 1646-1652.
12.   Timko, M. T.; Yu, Z.; Kroll, J.; Jayne, J. T.; Worsnop, D. R.; Miake-Lye, R. C.; Onasch, T. B.; Liscinsky, D.; Kirchstetter, T. W.; Destaillats, H.; Holder, A. L.; Smith, J. D.; Wilson, K. R., Sampling Artifacts from Conductive Silicone Tubing. *Aerosol Sci. Technol.* **2009,** Medium: ED; Size: 31.
13.   Ribuffo, D.; Lo Torto, F.; Giannitelli, S. M.; Urbini, M.; Tortora, L.; Mozetic, P.; Trombetta, M.; Basoli, F.; Licoccia, S.; Tombolini, V.; Cassese, R.; Scuderi, N.; Rainer, A., The Effect of Post-mastectomy Radiation Therapy on Breast Implants: Unveiling Biomaterial Alterations with Potential Implications on Capsular Contracture. *Materials Science and Engineering: C* **2015,** *57*, 338-343.
14.   Schneider, J.; Weimer, S.; Drewnick, F.; Borrmann, S.; Helas, G.; Gwaze, P.; Schmid, O.; Andreae, M. O.; Kirchner, U., Mass Spectrometric Analysis and Aerodynamic Properties of Various Types of Combustion-related Aerosol Particles. *Int. J. Mass Spectrom.* **2006,** *258*, 37-49.
15.   Yu, Y.; Liz Alexander, M.; Perraud, V.; Bruns, E. A.; Johnson, S. N.; Ezell, M. J.; Finlayson-Pitts, B. J., Contamination from Electrically Conductive Silicone Tubing during Aerosol Chemical Analysis. *Atmos. Environ.* **2009,** *43*, 2836-2839.